4-2016

Identification of the Zinc-oxygen Divacancy in ZnO Crystals

Maurio S. Holston
Air Force Institute of Technology

Eric M. Golden
Air Force Institute of Technology

Brant E. Kananen [*]
Air Force Institute of Technology

John W. McClory
Air Force Institute of Technology

Nancy C. Giles
Air Force Institute of Technology

See next page for additional authors

Recommended Citation

Holston, M. S., Golden, E. M., Kananen, B. E., McClory, J. W., Giles, N. C., & Halliburton, L. E. (2016). Identification of the zinc-oxygen divacancy in ZnO crystals. Journal of Applied Physics, 119(14), 145701. https://doi.org/10.1063/1.4945703

Identification of the zinc-oxygen divacancy in ZnO crystals

Cite as: J. Appl. Phys. **119**, 145701 (2016); https://doi.org/10.1063/1.4945703
Submitted: 17 February 2016 . Accepted: 28 March 2016 . Published Online: 11 April 2016

M. S. Holston, E. M. Golden, B. E. Kananen, J. W. McClory, N. C. Giles, and L. E. Halliburton

Identification of the zinc-oxygen divacancy in ZnO crystals

M. S. Holston,[1] E. M. Golden,[1] B. E. Kananen,[1] J. W. McClory,[1] N. C. Giles,[1] and L. E. Halliburton[2,a)]

[1]*Department of Engineering Physics, Air Force Institute of Technology, Wright-Patterson Air Force Base, Ohio 45433, USA*

[2]*Department of Physics and Astronomy, West Virginia University, Morgantown, West Virginia 26506, USA*

(Received 17 February 2016; accepted 28 March 2016; published online 11 April 2016)

An electron paramagnetic resonance (EPR) spectrum in neutron-irradiated ZnO crystals is assigned to the zinc-oxygen divacancy. These divacancies are observed in the bulk of both hydrothermally grown and seeded-chemical-vapor-transport-grown crystals after irradiations with fast neutrons. Neutral nonparamagnetic complexes consisting of adjacent zinc and oxygen vacancies are formed during the irradiation. Subsequent illumination below ~150 K with 442 nm laser light converts these $(V_{Zn}^{2-} - V_O^{2+})^0$ defects to their EPR-active state $(V_{Zn}^{-} - V_O^{2+})^+$ as electrons are transferred to donors. The resulting photoinduced S = 1/2 spectrum of the divacancy is holelike and has a well-resolved angular dependence from which a complete *g* matrix is obtained. Principal values of the *g* matrix are 2.00796, 2.00480, and 2.00244. The unpaired spin resides primarily on one of the three remaining oxygen ions immediately adjacent to the zinc vacancy, thus making the electronic structure of the $(V_{Zn}^{-} - V_O^{2+})^+$ ground state similar to the isolated singly ionized axial zinc vacancy. The neutral $(V_{Zn}^{2-} - V_O^{2+})^0$ divacancies dissociate when the ZnO crystals are heated above 250 °C. After heating above this temperature, the divacancy EPR signal cannot be regenerated at low temperature with light. © *2016 AIP Publishing LLC*. [http://dx.doi.org/10.1063/1.4945703]

I. INTRODUCTION

Native defects (i.e., vacancies, interstitials, and antisites) have been widely studied in ZnO crystals and are often invoked to explain optical and electrical results.[1–3] Isolated oxygen and zinc vacancies, in their paramagnetic singly ionized charge states, were initially identified in electron- and neutron-irradiated crystals using electron paramagnetic resonance (EPR).[4–15] For the oxygen vacancy, resolved hyperfine lines from the four adjacent ^{67}Zn nuclei provided definitive evidence that the correct assignment was made.[9] In the case of the zinc vacancies, analysis of their *g* matrices[16] and the presence of axial and nonaxial positions of the unpaired spin on adjacent oxygen ions allowed detailed models of the ground states to be established. Recently, positron annihilation spectroscopy has also been used to characterize isolated zinc vacancies and zinc-vacancy-related complexes in ZnO.[17–25]

After isolated monovacancies, the most likely native defect to occur in ZnO crystals is a divacancy. These could be either oxygen-oxygen (O-O) divacancies, zinc-zinc (Zn-Zn) divacancies, or zinc-oxygen (Zn-O) divacancies. Of these, the Zn-O divacancy is expected to have the smallest formation energy[26,27] because it combines an acceptor and a donor in a neutral close-associate pair. Many of the recent studies of ZnO have focused on the properties of thin films and nanoparticles, and it is here where the Zn-O divacancies may play an especially important role (as a result of their location near a surface). Isolated zinc and oxygen vacancies may be formed during the growth/synthesis process or during post-growth treatments at high temperatures in reducing or oxidizing atmospheres, and it is reasonable to expect that Zn-O divacancies are also generated. By creating these divacancies, individual zinc-vacancy acceptors and oxygen-vacancy donors become passivated and thus the optical and electrical behaviors of the thin films or nanoparticles are changed.

Although frequently mentioned as an important defect in ZnO,[20,24,28–30] the Zn-O divacancy has been little studied. Until now, no direct spectroscopic signature has been assigned to this defect. Results from a comprehensive EPR investigation of the ground state of the Zn-O divacancy in ZnO are described in the present paper, thus rectifying this lack of information. With its high resolution and sensitivity, EPR is an especially appropriate experimental technique to study these native defects in ZnO.[31,32] The Zn-O divacancies were produced in our crystals during a neutron irradiation and are initially in a nonparamagnetic neutral charge state. Illumination at low temperature with near-band-edge laser light then converts the neutral divacancies to an EPR-active paramagnetic charge state by removing an electron. Determination of the *g* matrix (principal values and principal-axis directions) and consideration of possible charge states of divacancies before and after illumination allow us to assign the observed S = 1/2 EPR spectrum to the Zn-O divacancy. In the remainder of this paper, we refer to the neutral Zn-O divacancy as $(V_{Zn}^{2-} - V_O^{2+})^0$ and the singly ionized paramagnetic form of the divacancy as $(V_{Zn}^{-} - V_O^{2+})^+$.

The EPR spectrum reported in the present paper has been previously observed in electron-irradiated single crystals of ZnO. Schallenberger and Hausmann,[33] in an early study, suggested that the responsible paramagnetic defect was a Zn-Zn divacancy with both vacancies in an (0001) plane. They refer

a)Author to whom correspondence should be addressed. Electronic mail: Larry.Halliburton@mail.wvu.edu.

to the paramagnetic state as a $(V_{Zn}^{-})_2^{-}$ center with the implication that the divacancy is a nonparamagnetic $(V_{Zn}^{2-} - V_{Zn}^{2-})$ center after electron irradiation, but before illumination. However, prior to optical excitation at low temperature, a pair of doubly ionized zinc vacancies occupying adjacent zinc lattice sites is not expected to be energetically favorable (each vacancy would have an effective double negative charge and there would be a strong repulsive effect). The present paper proposes a different, and more realistic, defect model for the EPR spectrum reported by Schallenberger and Hausmann.[33]

II. EXPERIMENTAL

The ZnO crystals used in the present investigation were grown by the seeded-chemical-vapor-transport (SCVT) method at Eagle-Picher (Miami, Oklahoma) and by the hydrothermal (HT) method at Tokyo-Denpa (Japan). Approximate dimensions of the EPR samples were $2.5 \times 4.0 \times 0.5\,\mathrm{mm}^3$. The neutron irradiations were performed at the Ohio State University Nuclear Reactor Laboratory (Columbus, OH). This is a pool-type reactor operating at a maximum power of 450 kW. The ZnO crystals were placed in the central irradiation facility of the reactor where the total neutron flux was $\sim 2.1 \times 10^{13}$ neutrons $\mathrm{cm}^{-2}\,\mathrm{s}^{-1}$ and the thermal neutron flux was $\sim 1.3 \times 10^{13}\,\mathrm{cm}^{-2}\,\mathrm{s}^{-1}$. Irradiation times ranged from 1.5 to 20 h. The temperature of the crystals was not measured during the neutron irradiations, but the survival of zinc vacancies produced by the high-energy neutrons suggests that it was less than 150 °C. After removal from the reactor, the ZnO crystals remain radioactive for extended periods of time. Absorption of thermal neutrons by ^{64}Zn nuclei (48.3% natural abundance) creates ^{65}Zn nuclei ($^{64}\mathrm{Zn} + \mathrm{n} \rightarrow {}^{65}\mathrm{Zn} + \gamma$). The newly formed ^{65}Zn nuclei then slowly decay to ^{65}Cu nuclei (the half-life of ^{65}Zn is 244 days).[34] Production of ^{65}Zn nuclei and the related activity can be significantly reduced in future neutron irradiations by using Cd to shield the ZnO crystals from thermal neutrons (Cd shielding was not used in our present irradiations).

A Bruker EMX spectrometer operating at ~9.40 GHz was used to take EPR data while an Oxford helium-gas flow system controlled the sample temperature. Magnetic field values were measured using a Bruker nuclear magnetic resonance (NMR) teslameter. Corrections for the small differences in magnetic field between the sample and the probe tip were made using the known g values of the singly ionized oxygen vacancy in ZnO ($g_{||} = 1.9945$ and $g_{\perp} = 1.9960$).[9] Vacancies were converted to their paramagnetic charge states by illuminating the neutron-irradiated crystals at low temperature in the microwave cavity with 442 nm light from a He-Cd laser. The energy of these photons is less than the optical band gap of ZnO.

The ZnO crystals are hexagonal (point group $6mm$ and space group $P6_3mc$) with $a = 3.242$ Å, $c = 5.188$ Å, and $u = 0.3819$.[35] As is customary, we use four indices [hkil] to specify directions and planes (the first three indices refer to the lattice vectors $\mathbf{a_1}$, $\mathbf{a_2}$, and $\mathbf{a_3}$ in the basal plane and the fourth index refers to the $\mathbf{c}$ lattice vector). The sum (h + k + i) is always zero in order to easily identify equivalent directions and planes. Two directions indexed by [hki0] and [h′k′i′0] are orthogonal when $\mathrm{hh}' + \mathrm{kk}' + \mathrm{ii}' = 0$. Figure 1(a) is a projection of the crystal on the (0001) plane. Specific directions referred to in the present paper are identified. Figures 1(b) and 1(c) are projections on the (2 $\bar{1}\,\bar{1}$ 0) and (10 $\bar{1}$ 0) planes, respectively.

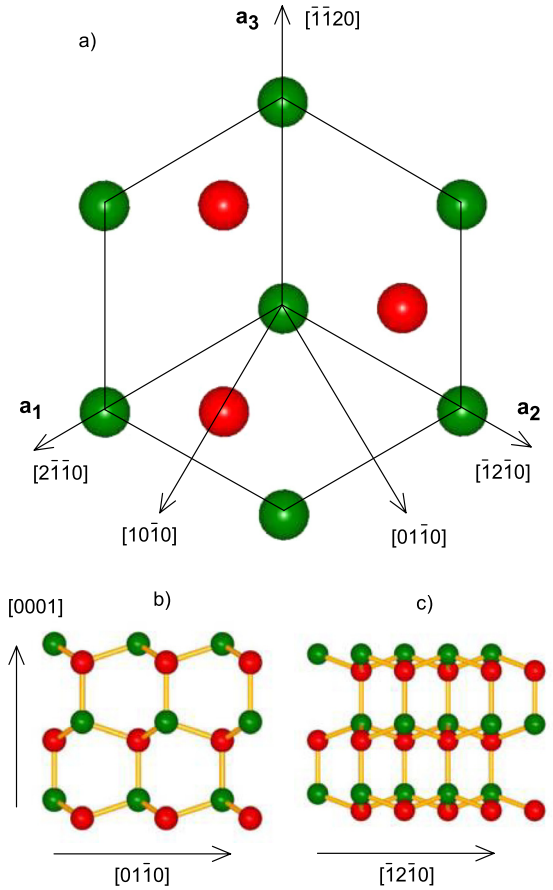

FIG. 1. Hexagonal (wurtzite) structure of ZnO crystals. Oxygen ions are red and zinc ions are green. (a) The basal plane (looking back along the [0001] direction). The three oxygen ions are behind the plane containing the seven zinc ions. The $\mathbf{a_1}$, $\mathbf{a_2}$, and $\mathbf{a_3}$ lattice vectors are in the basal plane. (b) The a plane (looking back along the [2 $\bar{1}\,\bar{1}$ 0] direction). (c) The m plane (looking back along the [10 $\bar{1}$ 0] direction).

III. RESULTS

A. EPR spectra

Figure 2 shows the photoinduced EPR spectrum from a neutron-irradiated SCVT-grown ZnO crystal (a nearly identical EPR spectrum was also present in the neutron-irradiated HT-grown ZnO crystal). These data in Fig. 2 were obtained at 37 K with the magnetic field aligned along the [0001] direction (i.e., the c axis). Laser light (442 nm) was incident on the crystal while the spectrum was recorded. There were no EPR signals present in this field region before illumination. The dominant EPR signal in Fig. 2, appearing near 335.24 mT, was first observed, and given the label S, by Leutwein and Schneider.[7] They did not propose a model for the responsible defect. In the present paper, we assign this signal to the singly ionized paramagnetic charge state of the Zn-O divacancy, i.e., the $(V_{Zn}^{-} - V_O^{2+})^{+}$ center. For this [0001] orientation of magnetic field, the g value of the divacancy signal is $g_c = 2.0037$. Other prominent features in Fig. 2 are the singly ionized oxygen vacancy (i.e., the V_O^{+}

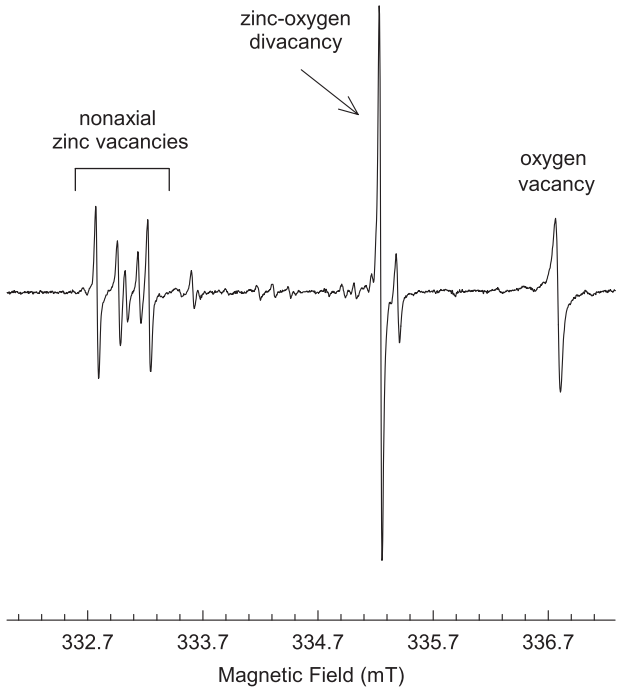

FIG. 2. EPR spectrum from a neutron-irradiated SCVT-grown ZnO crystal. These data were acquired at 37 K with the magnetic field along the [0001] direction and a microwave frequency of 9.4016 GHz. The crystal was illuminated with 442 nm laser light while the spectrum was taken. Signals from the zinc vacancies, the oxygen vacancy, and the Zn-O divacancy are present.

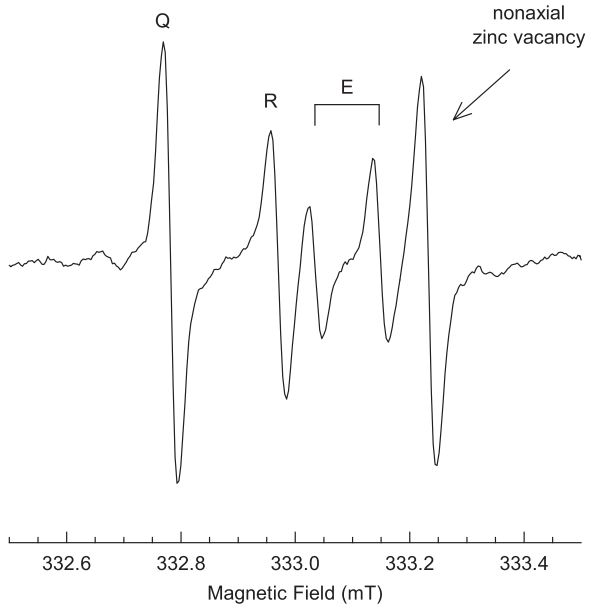

FIG. 3. Expanded view of the low-field region of Fig. 2 showing the EPR signals from isolated nonaxial zinc vacancies and E, R, and Q centers. These latter three defects have a zinc vacancy as the central component of their models. The magnetic field is along the [0001] direction.

center) near 336.79 mT, a less intense line near 335.40 mT just to the high-field side of the $(V_{Zn}^{-} - V_{O}^{2+})^{+}$ line, and a set of five lines near 333.0 mT. Additional information about the line near 335.40 mT is provided in Section III D. The EPR signals recently reported by Son *et al.*[36] and Stehr *et al.*,[37] and attributed to zinc-vacancy-related defects, were not present, with or without illumination at low temperature, in either the SCVT- or the HT-grown ZnO crystals after our neutron irradiations.

The five light-induced EPR lines in the lower magnetic field region in Fig. 2 are shown more clearly in Fig. 3. The single line at 333.23 mT in Fig. 3 is due to the isolated singly ionized nonaxial zinc vacancy.[5–7] In this defect, the hole is localized on one of the three equivalent basal-plane oxygen ions and there is no nearby perturbing entity. The related isolated singly ionized axial zinc vacancy was not observed in our neutron-irradiated crystals during an illumination at 37 K with 442 nm laser light. Earlier investigators also reported not seeing an EPR signal from axial zinc vacancies.[5,7] The existence of axial zinc vacancies, however, is well established[6,8] (the reason for the difficulty in observing their EPR signal is related to the fact that having the hole on one of the nonaxial oxygen neighbors is energetically more favorable than having the hole on the axial oxygen neighbor). Axial zinc vacancies are reported to have a g value of 2.0024 when the magnetic field is along the [0001] direction.[6] Thus, the EPR signal with $g_c = 2.0037$ in Fig. 2, and that we assign to the $(V_{Zn}^{-} - V_{O}^{2+})^{+}$ divacancy, is not due to isolated axial zinc vacancies. When the magnetic field is rotated away from the [0001] direction toward the [2 $\bar{1}\bar{1}$ 0] direction, the angular dependence of this line at $g_c = 2.0037$ shows even more clearly that it does not represent an isolated axial zinc vacancy. At 37 K, a splitting into several lines occurs during the rotation, as expected for the $(V_{Zn}^{-} - V_{O}^{2+})^{+}$ divacancy. The isolated axial zinc vacancy would remain one line that shifts to lower field during this rotation.

The closely spaced pair of lines labeled E and centered at 333.09 mT in Fig. 3 were initially reported by Evans *et al.*[14] A small hyperfine interaction with one proton causes the doublet in this E center and the proposed model for the defect is a zinc vacancy with a hole localized on a nonaxial oxygen neighbor and an OH^{-} molecular ion replacing one of the remaining three oxygen neighbors. The lines labeled R and Q in Fig. 3 represent two defects that were initially reported by Leutwein and Schneider.[7] These $S = 1/2$ centers have no resolved hyperfine splittings. Their g values indicate that they are both due to a hole localized at a nonaxial oxygen neighbor of a zinc vacancy. We suggest that these zinc-vacancy defects (R and Q) each have a nearby perturbing impurity, for example, an Al^{3+} or a Ga^{3+} ion on a Zn^{2+} site adjacent to the zinc vacancy. Due to electrostatic repulsion, the positive hole and the positive impurity will be as far apart as possible (i.e., on opposite sides of the vacancy). This is expected to result in a small, and very likely unresolved, hyperfine interaction with the ^{27}Al or the ^{69}Ga and ^{71}Ga nuclei. A clear example of this type of weak unresolved EPR hyperfine behavior is seen in the Al-associated magnesium vacancy in MgO where V_{Mg}^{-} and $(V_{Mg}^{-} - Al_{Mg}^{3+})^{0}$ centers have nearly identical spectra.[38] Because of the small magnitude of its hyperfine interaction, the presence of Al^{3+} in the latter defect was only detected with electron-nuclear double resonance (ENDOR).[39,40] In Fig. 3, the g_c values of the zinc-vacancy-related signals (i.e., the nonaxial zinc vacancy and centers E, R, and Q) when the magnetic field is along the [0001] direction are 2.0158, 2.0166, 2.0174, and 2.0185, respectively.

B. Spin-Hamiltonian parameters for the $(V_{Zn}^{-} - V_O^{2+})^{+}$ divacancy

The following spin Hamiltonian describes the S = 1/2 EPR spectrum associated with the $(V_{Zn}^{-} - V_O^{2+})^{+}$ charge state of the Zn-O divacancy in the neutron-irradiated ZnO crystals:

$$H = \beta \mathbf{S} \cdot \mathbf{g} \cdot \mathbf{B}. \quad (1)$$

Only an electron Zeeman term is needed since no hyperfine structure was observed for this defect. In general, six parameters define the g matrix (i.e., the three principal values and the three Euler angles that specify the principal-axis directions). A complete g matrix for the $(V_{Zn}^{-} - V_O^{2+})^{+}$ center was obtained by measuring the positions of EPR lines while rotating the direction of the magnetic field relative to the crystal axes. Data were taken every 10° in two high-symmetry planes, from [0001] to [2 $\bar{1}\bar{1}$ 0] and from [2 $\bar{1}\bar{1}$ 0] to [10 $\bar{1}$ 0]. These experimental results are represented by the discrete points in Fig. 4. The angular dependence of the spectrum when rotating the magnetic field from [0001] to [10 $\bar{1}$ 0] can be seen in Figure 6 in Ref. 33. There are 12 crystallographically equivalent orientations (i.e., sites) for the $(V_{Zn}^{-} - V_O^{2+})^{+}$ center in the hexagonal ZnO lattice. With the magnetic field along the [0001] direction, these 12 orientations are all magnetically equivalent and the EPR spectrum has one line. The 12 orientations separate into three distinguishable sets of four each when the field is along the [2 $\bar{1}\bar{1}$ 0] and [10 $\bar{1}$ 0] directions and three lines are present in the EPR spectrum. As shown in Fig. 4, there are six distinct lines in the spectrum when the field is rotated in the (01 $\bar{1}$ 0) and (0001) planes. For an arbitrary direction of magnetic field, there are 12 distinct lines in the spectrum (one for each orientation of the defect).

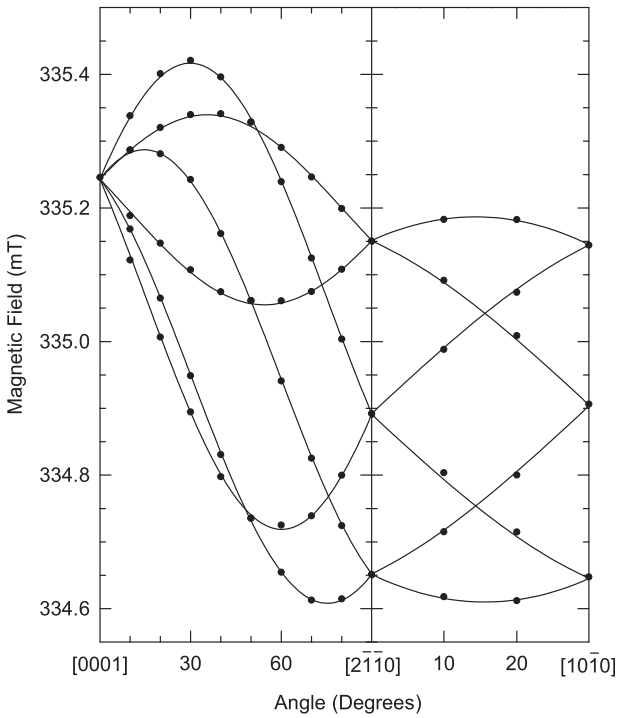

FIG. 4. Angular dependence associated with the g matrix of the $(V_{Zn}^{-} - V_O^{2+})^{+}$ divacancy. EPR line positions are plotted as a function of angle for rotations in the (0 1 $\bar{1}$ 0) and the (0001) planes. Solid curves were calculated using a microwave frequency of 9.4016 GHz and the set of g-matrix parameters in Table I. Discrete points are experimental results.

The spin Hamiltonian in Eq. (1) was rewritten in the form of a 2×2 matrix and then was repeatedly diagonalized as the six g-matrix parameters were systematically varied during a least-squares fitting. Input data were the 70 magnetic-field values (i.e., the discrete data points) in Fig. 4 and their corresponding microwave frequencies. Final best-fit values for these parameters are listed in Table I. The solid lines in Fig. 4 were computer-generated using these principal values and axis directions. Good agreement between the discrete experimental points and the calculated curves in Fig. 4 verifies that the correct g matrix has been determined. In Table I, the three Euler angles describing the three principal-axis directions have been converted to (θ,ϕ) pairs. The polar angle θ is defined relative to the [0001] direction and the azimuthal angle ϕ is defined relative to the [10 $\bar{1}$ 0] direction with positive rotation from [10 $\bar{1}$ 0] toward [$\bar{1}$ 2 $\bar{1}$ 0] in the (0001) plane. The set of principal-axis directions in Table I corresponds to one of the 12 crystallographically equivalent orientations of the $(V_{Zn}^{-} - V_O^{2+})^{+}$ center. Principal-axis directions for the other 11 orientations of the defect can be obtained by applying rotations based on the symmetry elements of the crystal.

C. Model of the $(V_{Zn}^{-} - V_O^{2+})^{+}$ divacancy

Significant concentrations of zinc vacancies and oxygen vacancies are created in our ZnO crystals by momentum-conserving displacement events initiated by high-energy neutrons. After the irradiation, but before illumination with near-band-edge laser light at low temperature, the isolated zinc vacancies are in their doubly ionized charge state (V_{Zn}^{2-}) and the isolated oxygen vacancies are in their neutral charge state (V_O^{0}). (Vacancies in these charge states have no unpaired spins and cannot be observed with EPR.) The newly produced zinc vacancies are acceptors that provide compensation for shallow donors and the slightly deeper transition-metal-ion donors, thus lowering the Fermi level in the irradiated crystals.[41] Also, during the irradiation, $(V_{Zn}^{2-} - V_O^{2+})^{0}$ neutral divacancies are formed as a portion of the mobile zinc vacancies move to oxygen vacancies (the diffusion of these zinc vacancies is enhanced because the temperature of the crystal is most likely well above 100 °C during the irradiation). In agreement with the computational

TABLE I. Principal values and principal axes of the g matrix for the singly ionized $(V_{Zn}^{-} - V_O^{2+})^{+}$ divacancy in a ZnO crystal. These results were obtained from the EPR angular dependence in Fig. 4. Estimated error limits are ±0.0002 for the g values and ±1.0° for the angles.

		Principal axes	
Principal values		θ (deg)	ϕ (deg)
g_1	2.00796	109.2	68.4
g_2	2.00480	58.2	145.9
g_3	2.00244	38.4	4.4

results of Shin and Kim[26] and Bang *et al.*,[27] the electronic structure of the neutral divacancy in ZnO is best viewed as a combination of a V_{Zn}^{2-} and a V_O^{2+} (i.e., two electrons are transferred from the oxygen vacancy to distant acceptors as the V_{Zn}^{2-} and V_O^0 centers approach each other). The paramagnetic state $(V_{Zn}^- - V_O^{2+})^+$ of the divacancy is then formed at temperatures below ~150 K when near-band-edge light (442 nm in our experiments) removes an electron from the oxygen ions adjacent to the zinc vacancy (i.e., this electron is "moved" to a donor). As long as the crystal remains at low temperature, the electron stays at the donor and the $(V_{Zn}^- - V_O^{2+})^+$ charge state of the divacancy is stable and observable with EPR. The $(V_{Zn}^- - V_O^{2+})^+$ center is paramagnetic with S = 1/2 because of the "hole" localized on the oxygen ions adjacent to the zinc vacancy, and the defect, as the label implies, is a combination of a V_{Zn}^- and a V_O^{2+}. A lack of observable hyperfine lines around the primary divacancy signals is evidence that the unpaired spin is on the oxygen ions (although ^{17}O nuclei have I = 5/2, they are only 0.038% abundant and are not usually seen in unenriched crystals). The electronic structure of the $(V_{Zn}^- - V_O^{2+})^+$ divacancy is similar to the isolated singly ionized zinc vacancy (V_{Zn}^-). The main difference being that the adjacent oxygen vacancy, with an effective double positive charge and no unpaired spins, acts as a significant perturbation on the V_{Zn}^- portion of the divacancy and reduces the local symmetry.

Small positive g shifts (g values greater than 2.0023 in Table I) for the $(V_{Zn}^- - V_O^{2+})^+$ center suggest that the unpaired spin, i.e., the hole, is primarily localized in a p orbital on an oxygen ion adjacent to the Zn vacancy. The direction of the unique axis of this p orbital must have its largest component along the [0001] direction since the g_c value of 2.0037 for the $(V_{Zn}^- - V_O^{2+})^+$ center is close to the $g_{||}$ value of 2.0024 for the isolated axial zinc vacancy. This expectation is verified by the results in Table I where the principal-axis direction corresponding to g_3 makes an angle of 38.4° with the [0001] direction in the crystal (g_3 is the g value closest to 2.0023 and thus the one that represents the unique direction of the p orbital). The deviation of the p orbital direction from [0001] is caused by the repulsive effect on the hole of the adjacent positive oxygen vacancy. A model for the $(V_{Zn}^- - V_O^{2+})^+$ center is illustrated in Fig. 5, where O_1, O_2, Zn_1, and Zn_2 all lie in the (1 $\bar{2}$ 1 0) plane. The Zn_1 and O_1 ions are missing and the unpaired spin (i.e., the hole) is localized primarily on the O_2 ion. In general, there are two possible configurations for the pair of vacancies that form the Zn-O divacancy, one where the vacancies are aligned along the [0001] direction and the other where they lie near the basal plane close to a [1 0 $\bar{1}$ 0] direction in a (1 $\bar{2}$ 1 0) plane. The orientation of the p orbital containing the unpaired spin (with its large component along the [0001] direction) suggests that the second configuration corresponds to our divacancy. In other words, the axis of the two vacancies must be close to the [10 $\bar{1}$ 0] direction (as shown in Fig. 5) in order for the p orbital to be aligned near the [0001] direction. Earlier computational studies have predicted that this [10 $\bar{1}$ 0] orientation of the Zn-O divacancy has the lowest energy.[26,27]

Although the unpaired spin in the $(V_{Zn}^- - V_O^{2+})^+$ center is localized in large part on the O_2 ion in Fig. 5, there may be

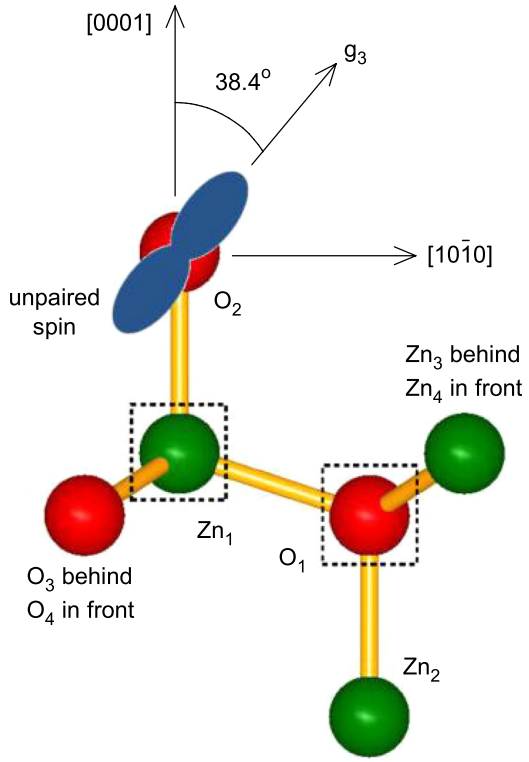

FIG. 5. Model of the paramagnetic $(V_{Zn}^- - V_O^{2+})^+$ divacancy shown in a projection on the (1 $\bar{2}$ 10) plane. The O_3 and Zn_3 ions are behind the plane and the O_4 and Zn_4 ions are in front of the plane. Vacancies are at the Zn_1 and O_1 positions and the unpaired spin (blue) is primarily localized in a p orbital on the O_2 ion with possible overlap onto the O_3 and O_4 ions.

a significant sharing of spin density with the O_3 and O_4 ions. Evidence to support this partial sharing with these two additional oxygen ions in the basal plane comes from the g_1 and g_2 principal g values in Table I (i.e., 2.00796 and 2.00480). These g values are analogous to $g_\perp$ for the isolated axial zinc vacancy. However, they represent smaller g shifts than the 2.0193 value of $g_\perp$ reported for the isolated axial zinc vacancy.[6] We anticipate that a partial sharing of the unpaired spin with the O_3 and O_4 ions is responsible for the reduced shifts found for g_1 and g_2. Also, we note that the p orbital occupied by the unpaired spin does not lie exactly in the (1 $\bar{2}$ 10) plane in Fig. 5 since the ϕ value in Table I for the 2.00244 principal value is 4.4° instead of 0° (specifically, the principal-axis direction associated with the 2.00244 principal value deviates from the midpoint of O_3 and O_4 by 4.4°). This suggests that the unpaired spin is not shared equally by the O_3 and O_4 ions since lattice distortion has reduced the local symmetry of the $(V_{Zn}^- - V_O^{2+})^+$ divacancy.

In the early stages of this study, we envisioned a quite different electronic structure for the paramagnetic charge state of the Zn-O divacancy formed during the low-temperature illumination of the neutron-irradiated crystals. Specifically, a photoinduced EPR spectrum was expected that would represent a doubly ionized zinc vacancy (V_{Zn}^{2-}) adjacent to a singly ionized oxygen vacancy (V_O^+). This $(V_{Zn}^{2-} - V_O^+)^-$ defect would have an unpaired spin localized on the three zinc ions neighboring the oxygen vacancy. After the neutron irradiation, but before the illumination at low temperature with laser light, this divacancy would be a

$(V_{Zn}^{2-} - V_O^0)^{2-}$ center and have no unpaired spins (the light then removes one electron and forms a paramagnetic defect). This $(V_{Zn}^{2-} - V_O^+)^-$ model, however, was quickly discarded because its EPR spectrum would have negative g shifts (principal values less than 2.0023) much like the isolated oxygen vacancies (V_O^+) and thus would not agree with the experimental results in Table I. Also, the EPR spectrum of a $(V_{Zn}^{2-} - V_O^+)^-$ divacancy would be expected to have well resolved hyperfine interactions with the ^{67}Zn nuclei adjacent to the oxygen vacancy,[9] but no ^{67}Zn hyperfine lines associated with the divacancy were detected in our spectra.

D. Thermal stability of the $(V_{Zn}^{2-} - V_O^{2+})^0$ divacancy

A pulsed anneal study was performed to obtain information about the dissociation temperature of the Zn-O divacancy, specifically the neutral nonparamagnetic $(V_{Zn}^{2-} - V_O^{2+})^0$ center, in the SCVT-grown ZnO crystal. This experiment consisted of a series of steps. First, the [0001] EPR spectrum from the $(V_{Zn}^- - V_O^{2+})^+$ center was recorded at 37 K after illuminating at this temperature with 442 nm laser light. The sample was then removed from the microwave cavity and heated in air to 100 °C in a bench-top furnace. After being held at this higher temperature for 5 min, the sample was returned to the microwave cavity, cooled to 37 K, and the $(V_{Zn}^- - V_O^{2+})^+$ center EPR spectrum was taken again after exposure to 442 nm light (the laser light repopulates the paramagnetic state of the divacancy). This incremental annealing process was repeated at 140 °C and again in 40 °C steps above 140 °C with 5 min holding times at each elevated temperature. After each step, the intensity of the EPR signal from the $(V_{Zn}^- - V_O^{2+})^+$ divacancy was recorded at the 37 K monitoring temperature. These thermal anneal results are shown in Fig. 6. The nonparamagnetic $(V_{Zn}^{2-} - V_O^{2+})^0$ divacancies initially formed during the neutron irradiation dissociate when the crystal is heated above approximately 250 °C. After heating above this temperature, the divacancy's EPR signal cannot be regenerated with light at low temperature.

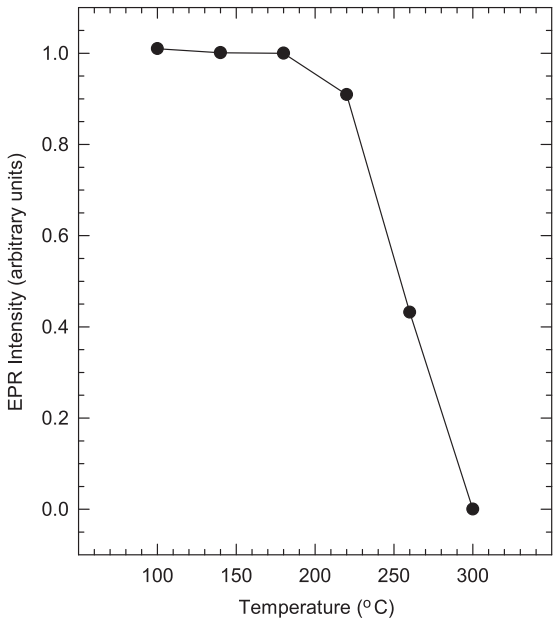

FIG. 6. Results of a pulsed anneal study (heating in air) show the thermal stability of the neutral $(V_{Zn}^{2-} - V_O^{2+})^0$ divacancy. The Zn-O divacancies dissociate when a neutron-irradiated crystal is heated above approximately 250 °C.

As the $(V_{Zn}^{2-} - V_O^{2+})^0$ divacancies disappear (i.e., dissociate) in the 200–300 °C range, the intensities of two of our other photoinduced EPR signals grow significantly. These two defects progressively increased in intensity following the 220, 260, and 300 °C anneal steps (described in the preceding paragraph). The spectra that increase are the E center represented by the doublet at 333.09 mT in Fig. 3 and the single line near 335.40 mT in Fig. 2. Their concentrations increased at the same rate during the anneal steps, thus suggesting that they have similar defect models. The E center has already been assigned to a zinc vacancy with the unpaired spin on a nonaxial oxygen neighbor and an OH^- ion replacing one of the remaining three oxygen neighbors.[14] By analogy, we tentatively assign the line at 335.40 in Fig. 2 to a zinc vacancy with the unpaired spin on an axial oxygen neighbor and an OH^- ion replacing one of the remaining three oxygen neighbors. A possible formation mechanism for these OH-related zinc vacancies is proposed. At temperatures between 200 and 300 °C, doubly ionized (V_{Zn}^{2-}) zinc vacancies are released from divacancies and thermally migrate though the lattice until they encounter OH^- ions. This results in nonparamagnetic $(V_{Zn}^{2-} - OH^-)^-$ centers when the zinc vacancy and the OH^- ion occupy adjacent lattice sites. Then, an exposure at 37 K to 442 nm light transfers an electron to a donor and forms the EPR-active $(V_{Zn}^- - OH^-)^0$ centers. The E center and the defect responsible for the line at 335.40 mT both have hydrogen (in the form of an OH^- ion) adjacent to the zinc vacancy. The primary difference between these defects is the position of the unpaired spin (on a nonaxial oxygen neighbor in one case and on an axial oxygen neighbor in the other case).

IV. SUMMARY

Electron paramagnetic resonance (EPR) is used to establish the ground-state model of the singly ionized Zn-O divacancy in bulk ZnO crystals. Neutral $(V_{Zn}^{2-} - V_O^{2+})^0$ divacancies are initially formed during a neutron irradiation. Subsequent illumination at temperatures below ~150 K with near-band-edge laser light then converts these divacancies into paramagnetic $(V_{Zn}^- - V_O^{2+})^+$ centers. A model for the $(V_{Zn}^- - V_O^{2+})^+$ divacancy is developed, based on the *g* matrix obtained from the angular dependence of the EPR spectrum. Positive *g* shifts suggest that this divacancy is holelike. In the proposed model, the unpaired spin (i.e., the hole) is located primarily in a *p* orbital on the axial oxygen neighbor of the zinc vacancy with significant overlap onto the remaining two oxygen neighbors of this vacancy. The line joining the zinc vacancy and the oxygen vacancy is close to a [10 $\bar{1}$ 0] direction (near the basal plane).

We anticipate that Zn-O divacancies may be especially important when native defects are located near the surface of bulk crystals or in nanoparticles.[42] Divacancies such as we describe, or slight variations because of their locations near or on the surface, could easily be formed when crystals or nanoparticles are exposed to various reducing atmospheres.

Once formed, these divacancies are expected to play a significant role in the observed optical and electrical behaviors of the material.

ACKNOWLEDGMENTS

The Air Force Institute of Technology received support for this work from the Defense Threat Reduction Agency through Grant Nos. HDTRA1-07-1-0008 and BRBAA08-I-2-0128. Views expressed in this paper are those of the authors and do not necessarily reflect the official policies or positions of the Air Force, the Department of Defense, or the United States Government.

[1]A. Janotti and C. G. Van de Walle, Rep. Prog. Phys. **72**, 126501 (2009).
[2]M. D. McCluskey and S. J. Jokela, J. Appl. Phys. **106**, 071101 (2009).
[3]H. Kaftelen, K. Ocakoglu, R. Thomann, S. Tu, S. Weber, and E. Erdem, Phys. Rev. B **86**, 014113 (2012).
[4]J. M. Smith and W. E. Vehse, Phys. Lett. A **31**, 147 (1970).
[5]A. L. Taylor, G. Filipovich, and G. K. Lindeberg, Solid State Commun. **8**, 1359 (1970).
[6]D. Galland and A. Herve, Phys. Lett. A **33**, 1 (1970).
[7]K. Leutwein and J. Schneider, Z. Naturforsch., A: Phys. Sci. **26**, 1236 (1971).
[8]D. Galland and A. Herve, Solid State Commun. **14**, 953 (1974).
[9]C. Gonzalez, D. Galland, and A. Herve, Phys. Status Solidi B **72**, 309 (1975).
[10]V. Soriano and D. Galland, Phys. Status Solidi B **77**, 739 (1976).
[11]V. A. Nikitenko, K. E. Tarkpea, S. F. Nikul'shin, and I. P. Kuz'mina, Zh. Prikl. Spektrosk. **47**, 834 (1987) [J. Appl. Spectrosc. **47**, 1198 (1987)].
[12]V. A. Nikitenko, Zh. Prikl. Spektrosk. **57**, 367 (1992) [J. Appl. Spectrosc. **57**, 783 (1992)].
[13]L. S. Vlasenko and G. D. Watkins, Phys. Rev. B **71**, 125210 (2005).
[14]S. M. Evans, N. C. Giles, L. E. Halliburton, and L. A. Kappers, J. Appl. Phys. **103**, 043710 (2008).
[15]L. A. Kappers, O. R. Gilliam, S. M. Evans, L. E. Halliburton, and N. C. Giles, Nucl. Instrum. Methods Phys. Res., Sect. B **266**, 2953 (2008).
[16]O. F. Schirmer, J. Phys. Chem. Solids **29**, 1407 (1968).
[17]F. Tuomisto, V. Ranki, K. Saarinen, and D. C. Look, Phys. Rev. Lett. **91**, 205502 (2003).
[18]Z. Q. Chen, M. Maekawa, S. Yamamoto, A. Kawasuso, X. L. Yuan, T. Sekiguchi, R. Suzuki, and T. Ohdaira, Phys. Rev. B **69**, 035210 (2004).
[19]F. Tuomisto, K. Saarinen, D. C. Look, and G. C. Farlow, Phys. Rev. B **72**, 085206 (2005).
[20]G. Brauer, W. Anwand, W. Skorupa, J. Kuriplach, O. Melikhova, C. Moisson, H. von Wenckstern, H. Schmidt, M. Lorenz, and M. Grundmann, Phys. Rev. B **74**, 045208 (2006).
[21]F. A. Selim, M. H. Weber, D. Solodovnikov, and K. G. Lynn, Phys. Rev. Lett. **99**, 085502 (2007).
[22]Z. Q. Chen, S. J. Wang, M. Maekawa, A. Kawasuso, H. Naramoto, X. L. Yuan, and T. Sekiguchi, Phys. Rev. B **75**, 245206 (2007).
[23]A. Zubiaga, F. Plazaola, J. A. García, F. Tuomisto, V. Muñoz-Sanjosé, and R. Tea-Zaera, Phys. Rev. B **76**, 085202 (2007).
[24]Z. Q. Chen, K. Betsuyaku, and A. Kawasuso, Phys. Rev. B **77**, 113204 (2008).
[25]G. Brauer, W. Anwand, D. Grambole, J. Grenzer, W. Skorupa, J. Čížek, J. Kuriplach, I. Procházka, C. C. Ling, C. K. So, D. Schulz, and D. Klimm, Phys. Rev. B **79**, 115212 (2009).
[26]E.-H. Shin and H. Kim, J. Korean Phys. Soc. **64**, 543 (2014).
[27]J. Bang, Y.-S. Kim, C. H. Park, F. Gao, and S. B. Zhang, Appl. Phys. Lett. **104**, 252101 (2014).
[28]S. A. Studenikin and M. Cocivera, J. Appl. Phys. **91**, 5060 (2002).
[29]R. Vidya, P. Ravindran, H. Fjellvåg, B. G. Svensson, E. Monakhov, M. Ganchenkova, and R. M. Nieminen, Phys. Rev. B **83**, 045206 (2011).
[30]S. Chattopadhyay, S. K. Neogi, P. Pandit, S. Dutta, T. Rakshit, D. Jana, S. Chattopadhyay, A. Sarkar, and S. K. Ray, J. Lumin. **132**, 6 (2012).
[31]J. A. Weil and J. R. Bolton, *Electron Paramagnetic Resonance: Elementary Theory and Practical Applications*, 2nd ed. (John Wiley and Sons, New York, 2007).
[32]J.-M. Spaeth and H. Overhof, *Point Defects in Semiconductors and Insulators: Determination of Atomic and Electronic Structure from Paramagnetic Hyperfine Interactions*, Springer Series of Materials Science Vol. 51 (Springer, Berlin, 2003).
[33]B. Schallenberger and A. Hausmann, Z. Phys. B: Condens. Matter **23**, 177 (1976).
[34]M. C. Recker, J. W. McClory, M. S. Holston, E. M. Golden, N. C. Giles, and L. E. Halliburton, J. Appl. Phys. **115**, 243706 (2014).
[35]J. Albertsson, S. C. Abrahams, and Å. Kvick, Acta Crystallogr., Sect. B: Struct. Sci., Cryst. Eng. Mater. **45**, 34 (1989).
[36]N. T. Son, J. Isoya, I. G. Ivanov, T. Ohshima, and E. Janzén, J. Phys.: Condens. Matter **25**, 335804 (2013).
[37]J. E. Stehr, K. M. Johansen, T. S. Bjørheim, L. Vines, B. G. Svensson, W. M. Chen, and I. A. Buyanova, Phys. Rev. Appl. **2**, 021001 (2014).
[38]L. E. Halliburton, L. A. Kappers, D. L. Cowan, F. Dravnieks, and J. E. Wertz, Phys. Rev. Lett. **30**, 607 (1973).
[39]W. P. Unruh, Y. Chen, and M. M. Abraham, Phys. Rev. Lett. **30**, 446 (1973).
[40]R. C. DuVarney and A. K. Garrison, Solid State Commun. **12**, 1235 (1973).
[41]Y. Jiang, N. C. Giles, and L. E. Halliburton, J. Appl. Phys. **101**, 093706 (2007).
[42]E.-H. Shin and H. Kim, J. Korean Phys. Soc. **66**, 625 (2015).